THE NATURE OF X-RAY SOURCES IN THE ANDROMEDA GALAXY

by

Erika Marentes Nava, B.S.

A thesis submitted to the Graduate Council of
Texas State University in partial fulfillment
of the requirements for the degree of
Master of Science
With a Major in Physics
August 2023

Committee Members:

Blagoy Rangelov, Chair

Aditya Togi

Andrea Banzatti

DEDICATION

Le quiero dedicar este trabajo a todos los que me apoyaron desde un principio. En especial, le quiero dedicar todo mi trabajo y esfuerzo a mi mamá Leticia Nava Barragán por siempre apoyarme y por siempre estar al pendiente de mí al pesar la distancia. Gracias, mamá por todo. Saludos a mi gente de Zacatecas, México. Ayer, hoy y siempre Zacatecana.

I want to dedicate this project to everyone that supported me from the beginning, especially to my mother Leticia Nava Barragán for always supporting me and looking out for me regardless of the distance barrier. Thank you, Mom, for everything. Shoutout to all my people from Zacatecas, Mexico. Always and forever, Zacatecana.

ACKNOWLEDGEMENTS

I want to acknowledge my committee, Dr. Aditya Togi, Dr. Andrea Banzatti, and Dr. Blagoy Rangelov, for accepting me as their mentee. I want to give a special thank you to Dr. Blagoy Rangelov for always being patient with me and guiding me every step of the way and continuing to do so. I appreciate the support I have received from all three members of my committee and the Department of Physics at Texas State University.

TABLE OF CONTENTS

Page

LIST OF TABLES……vii

LIST OF FIGURES……..viii

LIST OF ILLUSTRATIONS……..ix

LIST OF ABBREVIATIONS……..x

ABSTRACT……..xii

CHAPTER

I. INTRODUCTION……1

Andromeda Galaxy and Hubble Space Telescope……...1
Stellar Evolution……..3
Star Clusters……6
Binary Systems……6
X-ray Sources and Chandra……8
Extragalactic Astrophysics……10

II. METHODS……11

III. RESULTS……14

IV. CONCLUSION & FUTURE WORK…….....……...24

REFERENCES……..25

LIST OF TABLES

Table **Page**

1. Sources per brick……...16

LIST OF FIGURES

Figure **Page**

1. Mosaic image taken by Hubble Space Telescope for the PHAT program……...2

2. Four images where the 23 Bricks are shown and divided…….....3

5. All 1280 X-ray data plotted…….....14

6. X-ray plot with all 799 sources contained within the bricks (1-23)……..15

7. Color color diagram of X-ray sources……...…17

8. Variability of x-ray sources based on flux, in this case using the broad energy band (0.5-7 keV)……..18

9. Cumulative XLF for our sources in M31……...…….…..18

10. Color magnitude diagram F275W – F336W vs F275W……...……19

11. Color magnitude diagram F475W – F814W vs F814W……...…19

12. Color magnitude diagram F110W - F160W vs F814W……20

13. Color magnitude diagram comparison F475W – F814W vs F814W……21

14. Cumulative curve for X-ray source and parent cluster……..22

LIST OF ILLUSTRATIONS

Illustration **Page**

1. Hertzsprung-Russell Diagram……4

2. Roche-Lobe overflow……8

LIST OF ABBREVIATIONS

Abbreviation	Description
M31	Messier 31
HST	Hubble Space Telescope
FOV	Field-of-view
PHAT	Panchromatic Hubble Andromeda Treasury
Arcsec	Arcseconds
ACS	Advanced Camera for Surveys
WFC3	Wide Field Camera 3
μm	Micrometer
nm	Nanometer
NS	Neutron Star
BH	Blackhole
XRB	X-ray Binary
HMXB	High mass X-ray binary
LMXB	Low mass X-ray binary
CXO	Chandra X-ray Observatory
LETG	Low Energy Transmission Grating
HETG	High Energy Transmission Grating
ACIS	Advanced CCD Imaging Spectrometer
keV	Kiloelectvolts
XLF	X-ray Luminosity Function
Myr	Million years

RA	Right Ascension
Dec	Declination

ABSTRACT

Using the Panchromatic Hubble Andromeda Treasury (PHAT) Program and Chandra X-Ray Observatory, we have acquired archival data from ~1/3 of Andromeda Galaxy to study the properties of the X-ray sources. Only a small fraction (~1/3) of the X-ray sources within Andromeda have been classified. We determined a total of 799 x-ray sources with 781 of them containing more than one counterpart. We present preliminary analysis of the archival data including color-magnitude diagrams, x-ray spectral analysis, and theoretical modeling that help us determine what these sources are.

I. INTRODUCTION

Andromeda Galaxy and Hubble Space Telescope

The closest galaxy to ours is the Andromeda Galaxy or M31 located ~2 million light-years away from Earth. Since it is the closest galaxy to ours, it is the perfect candidate to study stellar and galaxy evolution. However, since M31 is nearby, the angular size is very large (over 2 degrees), which makes it hard to study with modern telescopes such as the HST, as it has a very small field-of-view compared to the size of M31. Therefore, researchers have been studying only parts of M31 in detail. Studying extragalactic stellar populations is only possible with a powerful telescope such as HST. Smaller telescopes, which can map M31 easily, lack the angular resolution necessary to resolve individual stars. On the other hand, the smaller FOV of HST makes it very expensive to observe the entire Andromeda galaxy. The PHAT program was carried out, mapping this area of M31 (Figure 1). With a total of 7,398 exposures, Hubble has created the largest mosaic to date. Within this section of M31, Hubble has exposed over 100 million stars and thousands of star clusters.

HST was launched on April 24, 1990, as the most powerful telescope at the time. This telescope can detect galaxies from 13.4 billion light-years using wavelengths from ultraviolet to the near-infrared with a field of view of 202-by-202 $arcsec^2$.

There are two primary cameras installed on Hubble: ACS and the WFC3. Both cameras were used for this project.

Figure 1. Mosaic image taken by Hubble Space Telescope for the PHAT program. This image shows the region studied under the PHAT program.

The PHAT is a multi-cycle program that focuses on studying ~1/3 of M31 using six different filters under Hubble Space Telescope. The filters used to study M31 are the following: F275W+F336W, F475W+F814W, and F110W+F160W. F represents filter, the number represents the wavelength (F275W+F336W in μm, F475W+F814W in nm, and F110W+F160W in 10^{-2} μm), and the W represents wide band. F275W+F336W are the ultraviolet filters, F475W+F814W are the optical filters, and F110W+F160W are the near-infrared filters. These observations were done using Hubble's Wide Field Camera 3 for ultraviolet and near-infrared imaging and Advanced Camera for Surveys used to image in the optical.

The complete survey consists of an irregular, rectangular area with most of the bulge, or center of the galaxy, being covered by the survey as shown in figure 2. The region spreads from

the bulge to the northeast of the galaxy. To receive accurate data, the ~1/3 of M31 has been divided into twenty-three sub-areas known as bricks in which data has been continuously acquired from. These bricks are divided into rectangular shapes where the middle portion is compiled by a small fraction of six bricks. Each brick is named as Brick with the number following it. Brick 1 is located at the bulge and goes to the extent of the axis to Brick 23 (see Figure 2).

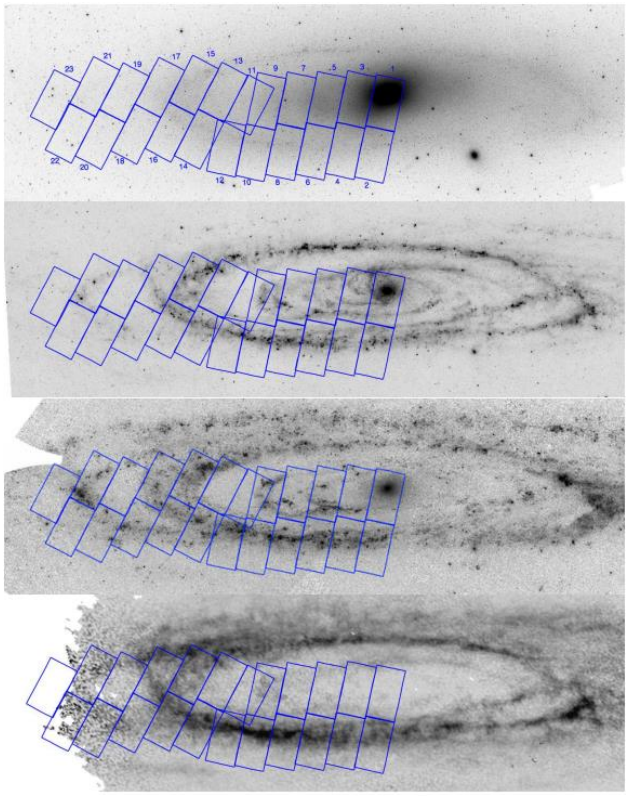

Figure 2. Four images where the 23 Bricks are shown and divided. From top to bottom: Spitzer 3.6μ (Barmby et al. 2006), Spitzer 24μ (Gordon et al. 2006), GALEX FUV image (Thilker et al. 2005), and Westerbork HI image (Brinks & Shane 1984).

Stellar Evolution

An important process to understand the ~1/3 of M31 is by studying stellar evolution. Each star goes through different stages during their lifetime. A very useful way to illustrate the

different stages of stars is known as The Hertzsprung-Russell Diagram.

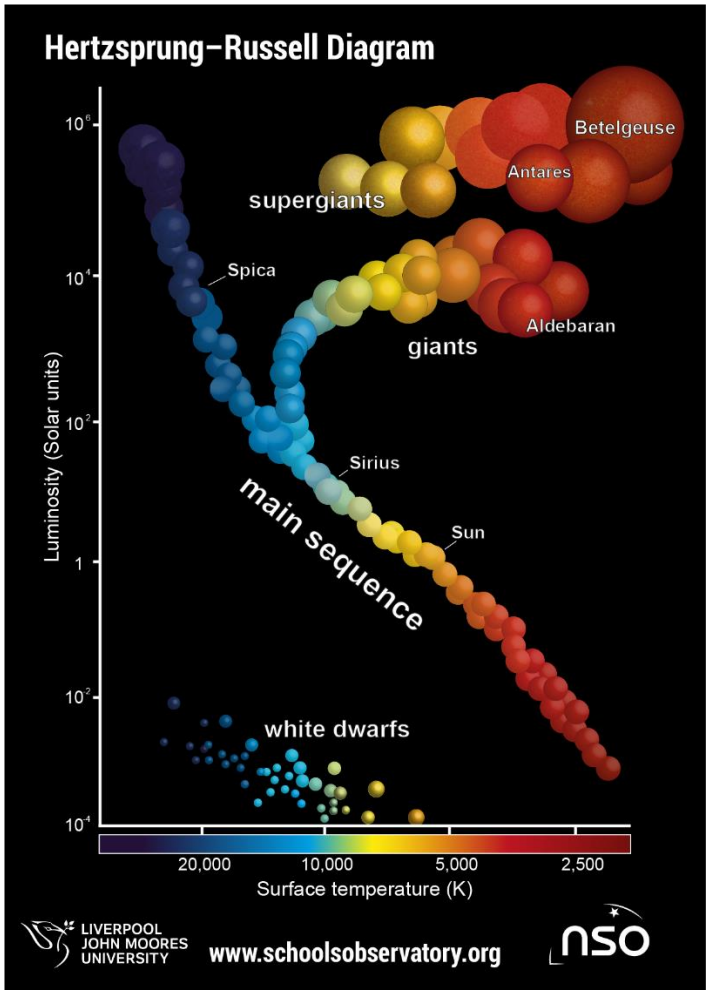

Figure 3. Hertzsprung-Russell Diagram. Surface temperature in the x-axis and luminosity in the y-axis. Names of popular stars are displayed in the diagram.

The Hertzsprung-Russell Diagram is described by the star's absolute magnitude, spectral class, luminosity, and effective temperature. Absolute magnitude is defined as the magnitude of brightness if the star is to be at 10pc. This can be found by using the following equation:

$$m - M = 2.5log_{10}\frac{d^2}{10^2}$$

where m is apparent magnitude and d is the actual distance of the star from Earth in pc. The apparent magnitude is defined as the apparent brightness of the star in the sky. Spectral class is

defined as the classification of a star based on their surface temperature. The spectral classes are O, B, A, F, G, K, M where the order of the spectral class decreases based on surface temperature. Luminosity is the quantity used to measure how much total energy is released by a star per second. In Figure 3, the luminosity of all stars is compared to our Sun where the sun has luminosity of 3.8×10^{26} W. Finally, the effective temperature is the surface temperature of the star or the blackbody radiation.

Based on these stellar quantities, stars are grouped into the following main categories: main sequence, red giants, super-giants, white dwarfs as shown in Figure 3. Most stars lie in the main sequence which is where most of their life is spent. The more massive main sequence stars are in the upper left corner of the band decreasing in mass from left to right. Once a main sequence star runs out of hydrogen through the process of fusion, they begin to evolve to the next stage: red giant or super-giant depending on their mass. The upper left corner of the main sequence will evolve to a super-giant while the lower evolve to a red giant. During this stage of their lifetime, the star begins the process of dying. Depending on the mass of the star, it will form a planetary nebula (for low mass stars), which is gas and dust from the outer layers of the red giant or undergo supernova (for massive stars). What is left in the planetary nebula is a white dwarf. When a star undergoes supernova, its final stage is a NS, the collapsed core of a supermassive star, or a BH.

The blue stars located on the left side of the Hertzsprung-Russell Diagram are the hotter and more massive stars. The more massive and hotter stars die faster than those cooler and redder. For the most massive and hotter stars, their final stage is a BH. Regardless of what evolution path a star may take, the left-over gas and dust from a supernova or planetary nebula can enrich nearby stellar nurseries. New stars are born, and the life cycle of a star continues.

Star Clusters

Most stars are grouped together in clusters. There are two different types of clusters: globular clusters and open clusters. Globular clusters consist of stars grouped together from thousands to millions of stars that are gravitationally bound together. Stars located in globular tend to be population II stars which ranges between 11 billion to 13 billion years. Many stars in globular clusters range the same age with the same composition. In the other hand, open clusters are loosely groups of stars, mainly young stars. Open clusters range in age but often contain young stars. Extragalactic star clusters are often blended (individual stars cannot be resolved), however, we can still determine the mass and age of such clusters by comparing them to models. This is a useful tool, which we will use in this work to investigate the nature of the X-ray sources in M31.

Binary Systems

Within star clusters, many stars will be in a binary system where two stars are orbiting around the system's center of mass. Most stars are in a binary system at which many are in a triple or higher multiple system. In fact, about 85% of stars are in a binary system or higher dimension. The dynamics of binary systems differ based on the type of stars that are in orbit. If the two stars are close together, they may be exchanging material from the companion star.

There are five types of binary systems: visual, spectroscopic, eclipsing, astrometric, and exotic. Binary systems are classified based on the method of detection.

1. Visual binaries are those that can be seen and are detected by a telescope. They tend to be close enough to Earth to be able to distinguish the stars individually. These types of stars are a few hundred astronomical units away that they do not exchange material.

2. Spectroscopic binaries are stars that cannot be visually resolved with telescopes. These types of binaries are detected using the spectrum of each individual star in the system. To confirm it is a binary system, the spectrum from one star must be redshifted and the other star must be blue shifted showing that they are in orbit.
3. Eclipsing binaries are those systems whose intrinsic luminosity changes. These types of stars are pulsating variable stars. The variation in brightness is due to the stars being aligned with Earth's point-of-view. When star B is behind star A, the intrinsic luminosity changes. Astrometric binaries are binaries detected by their proper motion. Proper motion is the position and motion of a celestial object in the sky. These observations are long-term since several measurements must be made.
4. Lastly, we have the exotic types of binary systems. This type of binary system consists of at least one NS or BH with a companion star, usually a main sequence star or red giant. Since both stars are close in distance, there is accreting material from the companion star onto the neutron star or black hole. The material is drawn from the companion star through Roche-Lobe overflow or stellar wind impact as shown in figure 4. Their period is usually 1.5 days or less. These types of exotic binaries are known as XRBs and consist of white dwarfs, NS, and BHs. These XRBs produce a high number of X-rays from material falling into the donor star, usually a regular star.

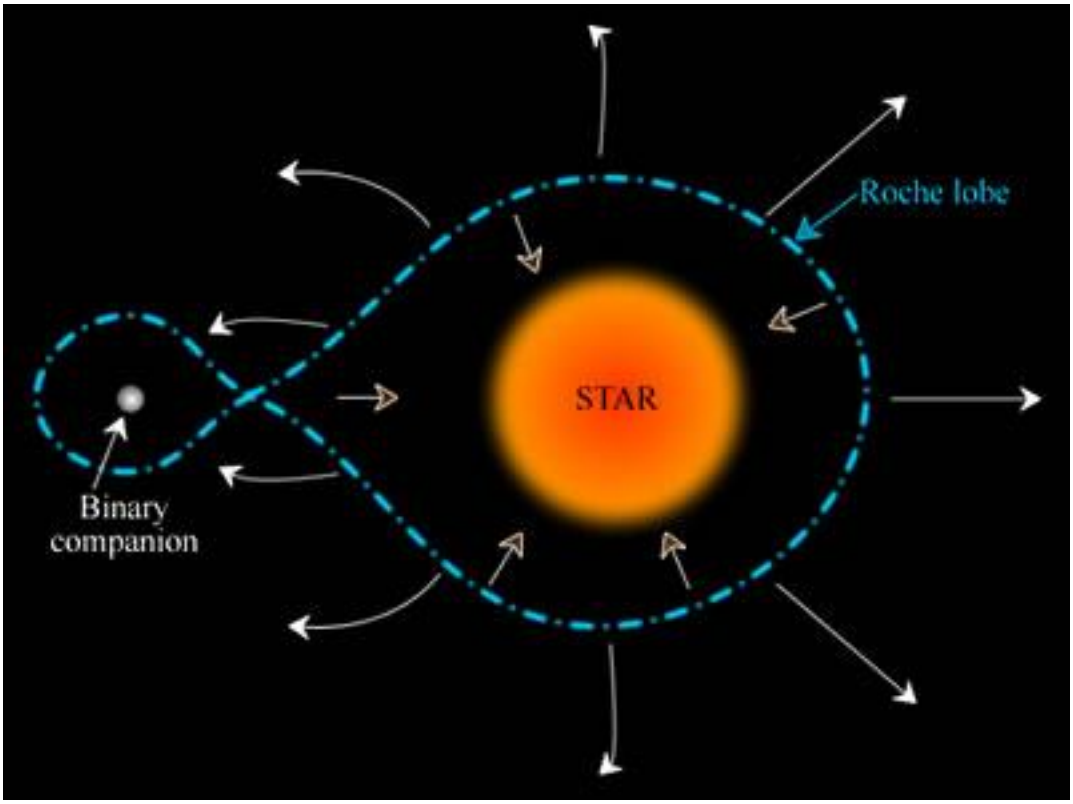

Figure 4. Illustration depicting a Roche-Lobe overflow.

X-ray Sources and Chandra X-ray Observatory

It is important to study celestial objects in X-rays because it can lead to a better understanding of the nature of the source. Such x-ray sources could be single stars (usually foreground stars), supernovas, and XRBs.

Single stars that produce the most amount of X-ray emission are O-type stars. These types of stars are the most massive and hottest stars in the main sequence. Due to how massive O-type stars are, they produce powerful stellar winds in which X-rays are emitted. Moreover, when the core collapses resulting in supernova, a vast number of X-ray photons are released.

XRBs are types of exotic binary systems. These types of binaries are considered closed since they are close enough to exchange matter. There are two types of X-ray binaries: HMXB

and LMXB.

A HMXB consists of a companion, an early-type star, that transfers material onto the compact object with its stellar winds. A LMXB does not have a companion which has strong stellar winds as a HMXB. However, the material from the companion star creates a region known as the Roche-lobe that surrounds the compact object as the material falls into the compact star. This orbiting material is gravitationally bounded with a critical point known as the langrage point. The nature of XRBs depends on the properties of the source, from the mass of the compact and companion object to the type of companion and compact object.

The current flagship X-ray telescope used to study x-ray emission is NASA's CXO. Launched in 1999, it is the most powerful X-ray telescope at the time. Chandra consists of mirrors placed parallel to the incoming X-ray photons. X-ray photons are focused on the focal plane before scattering onto the mirrors. Apart from the mirrors, X-ray photons are captured by several science instruments within Chandra. It contains two spectrometers, LETG and HETG. Both spectrographs diffract X-ray energy as it enters the detectors. The LETG consists of low energies between 0.07-0.15 keV whereas the HETG consists of higher energies between the range of 0.4-10 keV. In the focal plane, two instruments are focused on imaging and record data from the X-ray photons. These two instruments are known as HRC and ACIS.

Using Chandra's data, we focused on the different flux bands represented as

1. Flux_aper90_b (broad band): 0.5-7 keV
2. Flux_aper90_s (soft band): 0.5-0.7 keV
3. Flux_aper90_m (medium band): 1.2-2.0 keV
4. Flux_aper90_h (hard band): 2.0-7.0 keV.

Extragalactic Astrophysics

The Milky Way galaxy is by far the most studied galaxy. However, to understand the morphology, evolution, properties, and dynamics of galaxies, other galaxies must be studied. Extragalactic Astrophysics focuses on studying galaxies that are not our own like M31. Galaxies come in different sizes and shapes. The morphology of galaxies has been schemed based on three types of galaxies: elliptical, spiral, and irregular galaxies. Other types of galaxies not listed in the Hubble sequence are active galaxies and starburst galaxies.

Using the above parameters, to better understand the phenomenon of galaxies, studying the x-ray sources can give a deeper understanding of them. In this work, we study the nature of the X-ray sources in M31 that were observed by the PHAT program. We use the analysis of the X-ray and optical properties of the X-ray sources, as well as their relation to the star clusters in M31.

II. METHODS

We used archival data from HST and CXO. The data from HST was downloaded using the Barbara A. Mikulski Archive for Space Telescopes: an archive collection under The Space Telescope Science Institute. Using both data sets, we use the TOPCAT tool to cross match both data sets into one. With this information we can determine and learn more about the x-ray sources in the region.

Since the region of interest is divided into twenty-three bricks, we have created lines of code to identify each brick as its own. Moreover, with these lines of code, we were able to determine how many x-ray sources were found in each brick and then get a total of x-ray sources. This also helped us clean out sources not part of our region of interest.

Using our X-ray data and the Chandra Source Catalog, we determined the hardness ratios of our sources by using the hard-medium and medium-soft bands. This was calculated using the Chandra Source Catalog release 2 scheme:

$$HR_{xy} = \frac{F(x) - F(y)}{F(x) + F(y)}$$

where both $F(x)$ and $F(y)$ are both aperture fluxes (energy bands), x being the higher energy band and y being the lower energy band.

After obtaining the hardness ratio, we checked for X-ray variability of all our sources. We used the Gregory-Loredo Variability Probability and the Intra- Observation Variability Index which represents the highest value of the variable index. The range of the index [0,10] combines the Gregory-Loredo Variability probability and the light-curve
from the Gregory-Loredo analysis within 3σ and 5σ. The Gregory- Loredo Variability is used to detect time variability in x-ray sources. It consists of calculating the odds ratio, analyzing the light curve fractions, and assigning a variability index.

To understand the current evolution stage of these sources, we created color-magnitude diagrams using HST/ACS wfc updated filters and zero points, 2021 and HST/WFC 3 wide filters (UVIS/IR) updated filters and zero points stellar isochrones. The color-magnitude diagrams created were the following:

1. F275W – F336W vs F275W
2. F475W – F814W vs F814W
3. F110W – F160W vs F160W

We completed two sets of color magnitude diagrams. The first set of color magnitude diagrams were made using all optical matches (often their multiple counterparts to each X-ray source) within the 23 bricks and the second set of color magnitude diagrams were made using the true counterparts of the X-ray source. This means the second set of color magnitude diagrams contain less sources than the original color magnitude diagrams due to eliminating sources from the first set. To get the true counterpart of the X-ray sources, we had to use two different methods to find the true counterpart and compare both methods. The first method is using distance. The closest counterpart to the X-ray source is considered as the true counterpart. The second method is luminosity. By finding the brightest counterpart is considered as the true counterpart. Both methods were plotted to analyze and compare both plots. For the true counterpart using both methods, the color-magnitude diagram F475W – F814W vs F814W was used since both are optical filters with most sources shown.

We also used CDS source catalog to acquire a list of 1363 M31 PHAT star clusters de Meulenaer et al. 2017 to find the closest cluster for each X-ray source. De Meulenaer et al. 2017 selected a subsample of star clusters from Johnson et al. 2015 star cluster catalog based on high photometric accuracy to determine cluster age, mass, extinction, and metallicities. Visually, these

clusters were analyzed using ACS+WFC3 frames and accepted if visible using the PHAT main passbands (WFC3/F336W, ACS/F475W, and ACS/F814W).

III. RESULTS AND DISCUSSION

We have obtained a total of 1280 sources from the Chandra data set as shown in Figure 5; however, 799 of the X-ray sources are contained within the bricks as shown in Figure 6. Most of these sources are located closer to the nucleus.

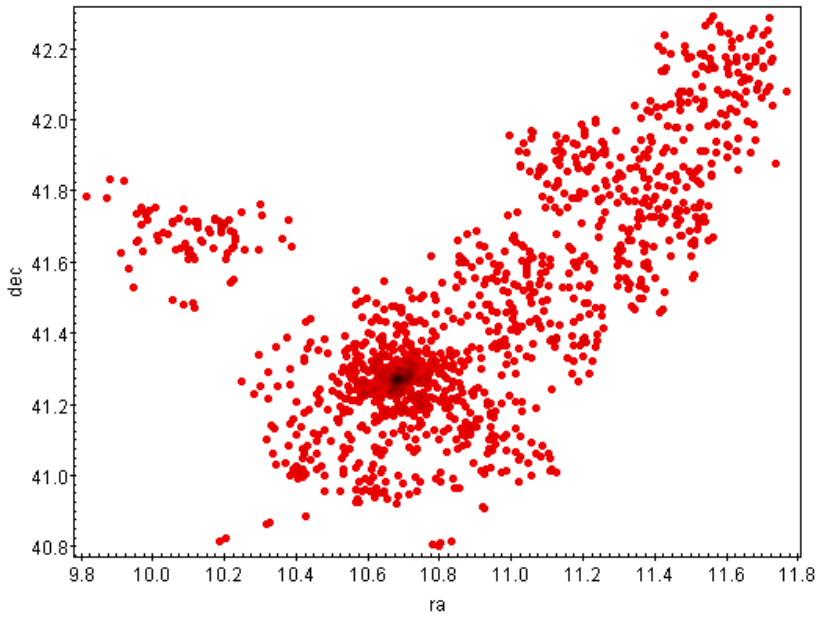

Figure 5. All 1280 X-ray data plotted with right ascension in the x-axis and declination in the y-axis. The units for this plot are in degrees. This plot was created using the TOPCAT tool.

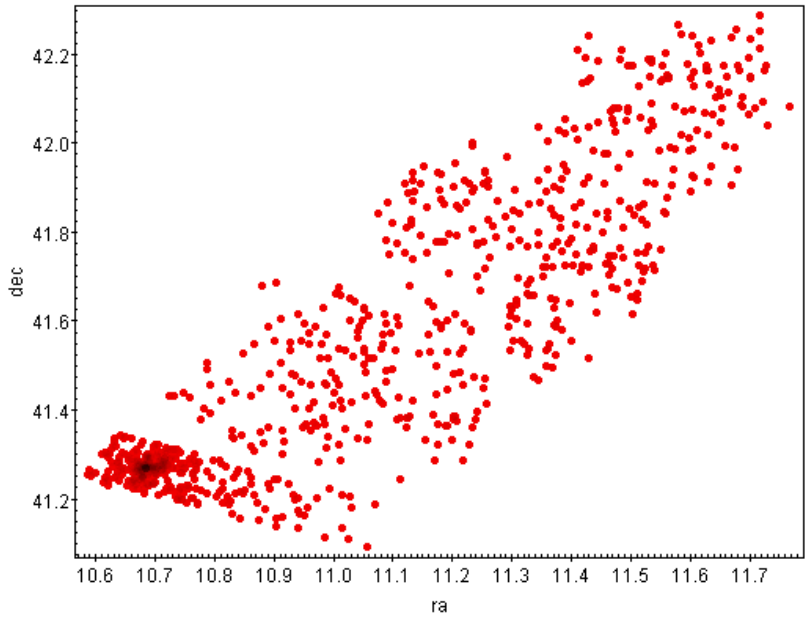

Figure 6. X-ray plot with all 799 sources contained within the bricks (1-23). Notice, most sources are closest to the nucleus (dark red). Refer to figure 2 for brick order. Units for this plot are in degrees. Used TOPCAT tool to create this plot.

We can determine this is accurate since theoretically most X-ray sources are found near the bulges of galaxies. A table has been created to determine how many X-ray sources are contained in each brick. This is found in Table 1.

Sources Per Brick

Table 1. This Table contains the number of X-ray sources found per brick. Recall, brick number 1 is located closest to the bulge of the galaxy. Refer to figure 2. We can determine from the table that brick 1 contains the largest fraction of X-ray sources with 275/799 and the brick with the least number of X-ray sources being brick number 19 with 0 X-ray sources.

Brick Number	Number of X-ray Sources	Brick Number	Number of X-ray Sources
1	275	13	27
2	35	14	42
3	17	15	38
4	9	16	28
5	31	17	16
6	34	18	44
7	35	19	0
8	16	20	18
9	17	21	33
10	25	22	8
11	16	23	9
12	26	TOTAL	799

Using our X-ray data, we determined the hardness ratios using hard color vs. soft color. Hard color is defined as high photon energies (5-10keV) and anything below 5keV is considered as soft color because of low photon energies. Most of the X-ray sources in M31 have too few total counts to allow us a proper spectral fitting analysis. We tried to use the X-ray colors of the sources to get some insight into their nature. Unfortunately, as seen from Figure 7, it is very difficult to determine the nature of the X-ray emission based on the basic X-ray color diagrams.

As we can conclude from our plot, our sources vary in different photon energies and do not follow, and model as shown in Figure 7.

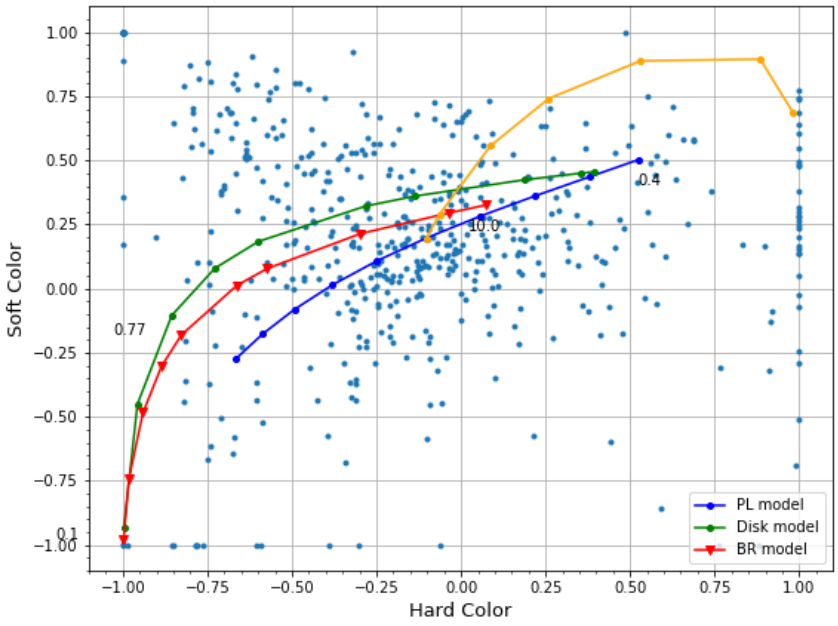

Figure 7. Color color diagram of X-ray sources. Hard minus medium vs. medium minus soft hardness ratios. In this figure, we have a comparison of the power law model (PL) in blue, disk blackbody model in green, and the absorbed bremsstrahlung model (BR).

Using Chandra's Source Catalog, we were able to obtain the X-ray variability of the sources (Figure 8). In Figure 8, the X-ray sources create a concave up plot. All our sources have different X-ray variability.

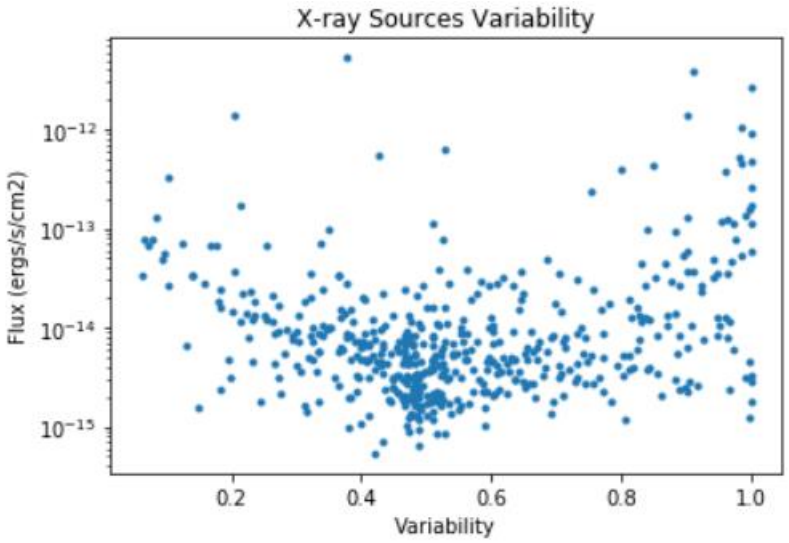

Figure 8. X-ray variability of x-ray sources based on flux, in this case using the broad energy band (0.5-7 keV).

Figure 9 shows the XLF of all 799 sources. The XLF can be approximated as a power law within a certain luminosity range. We fit a power law to the luminosity function with $\alpha = -1.7 \pm 0.1$ within the ~10^{35}-10^{38} erg/s range (the figure shown below is for Cumulative luminosity function). This is consistent with XLFs for other star-forming galaxies dominated by HMXBs.

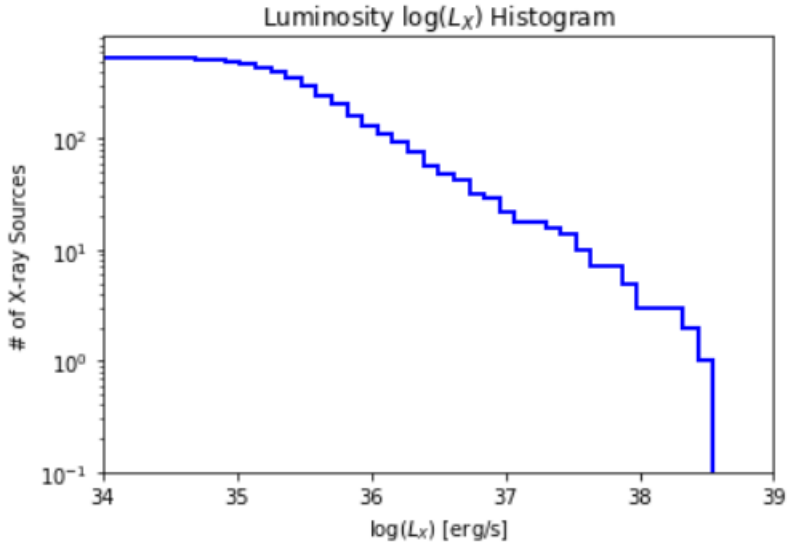

Figure 9. Cumulative XLF for our sources in M31.

Using the crossmatched data from HST and CXO, we have plotted three color magnitude diagrams to show the ages of our X-ray sources within the bricks and the evolutionary stage. Figure 11 contains the most sources, as expected, since this figure uses optical filters while Figure 10 contains the least number of sources.

Figure 10 shows that most, if not all, sources are passed the main sequence stage and are more evolved. All the sources in this figure fall between 10 million and 500 million years.

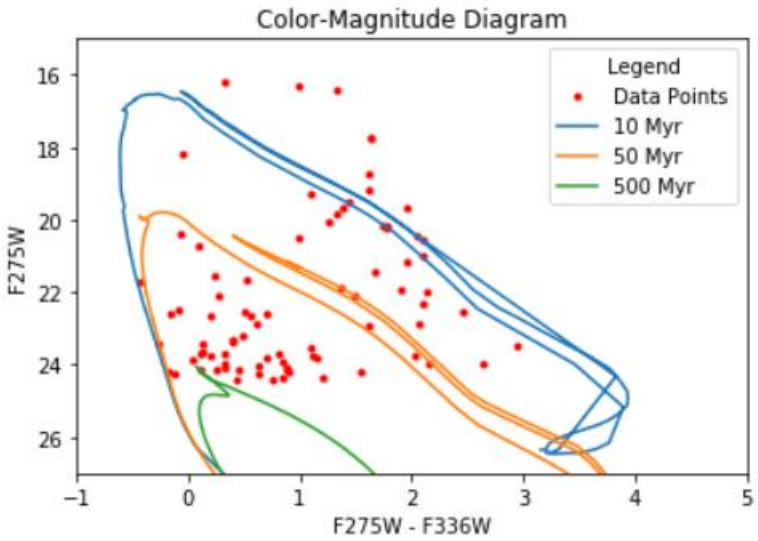

Figure 10. F275W – F336W color in the x-axis and F275W magnitude in the y-axis.

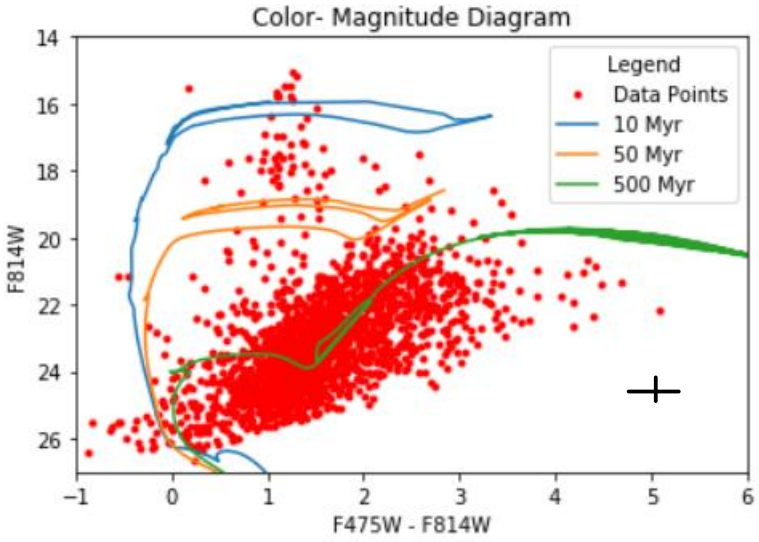

Figure 11. F475W – F814W color in the x-axis and F814W magnitude in the y-axis.

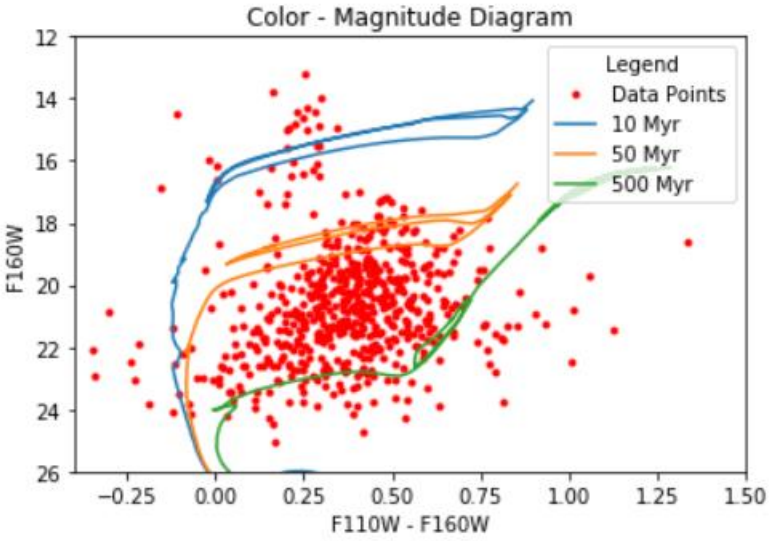

Figure 12. F110W - F160W color in the x-axis and F814W magnitude in the y-axis.

Figure 11 shows that most sources viewed in the optical are ~500 million years of age and are also evolved. Figure 12 shows most of our sources are between 50 million to 500 million years of age, also evolved.

781/799 X-ray sources contain at least one counterpart (observed in one or more filters).

Using the optical filters, we were able to model new color magnitude diagrams with the true counterpart by using both distance and luminosity methods. There are a total of 781 X-ray sources with true counterparts found by using the distance method and 653 X-ray sources with true counterparts using the luminosity method. Both methods have 242 common counterparts.

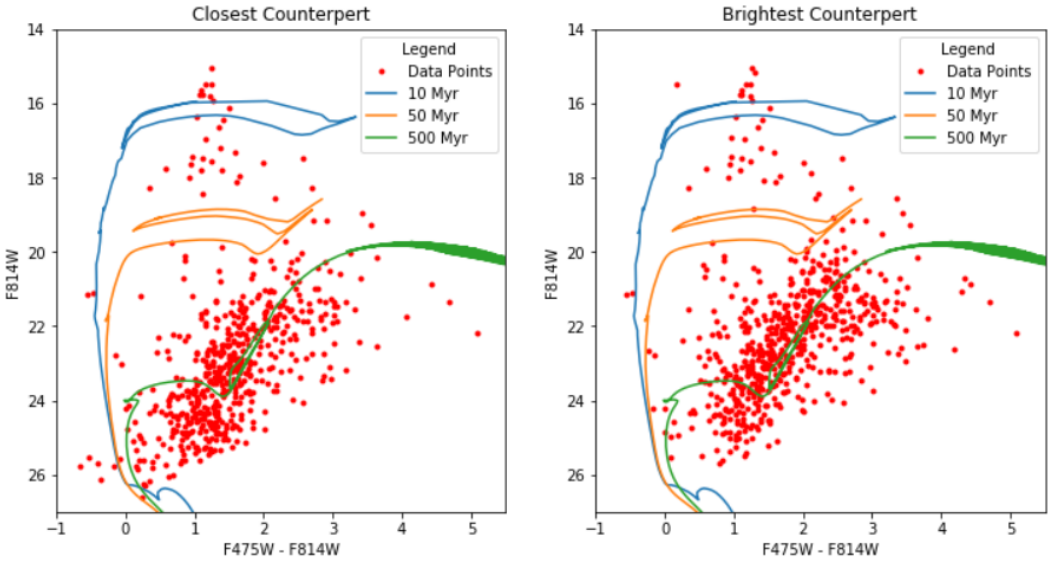

Figure 13. Color magnitude diagrams comparison: closest counterpart and brightness counterpart.

We compared both color-magnitude diagrams in Figure 12. We can conclude that most of our X-ray sources are around 500 million years with very few younger sources. Based on our findings, we can conclude that majority of the X-ray sources in M31 are XRBs, with a bit mixed population of HMXBs and LMXBs. We came to this conclusion because most X-ray sources are in the more evolved stages (red giant or super giant branch). Nevertheless, the HMXBs appear to be dominating the XRB population.

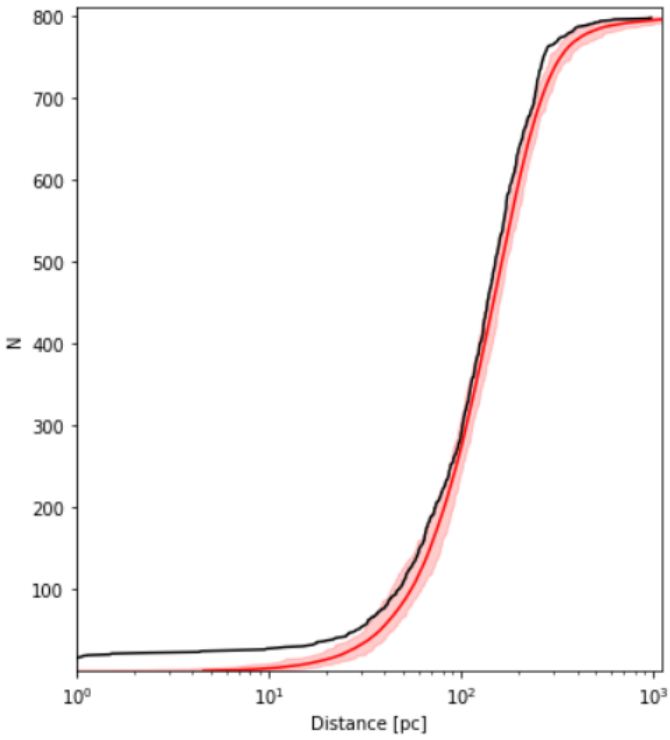

Figure 14. Cumulative curve. Red: simulated; black: real curve: red highlight: average.

We used the star cluster catalog published by de Meulenaer et al. 2017 to get more information about the nature of the X-ray sources. Since most stars form in star clusters, it is only natural to expect that the XRBs form in clusters as well. The XRBs found in the "filed" (outside of star clusters) are likely ejected due to dynamical interactions or by receiving a "kick" during the asymmetric supernova explosion of the primary star. To test this hypothesis, we assume that the closest cluster to each X-ray source is the parent cluster. Figure 13 shows the cumulative distribution between each X-ray source and its parent (closest) cluster candidate. Note that these are projected distances as the real 3-dimential position within M31 of the clusters and X-ray sources is unknown. For comparison, we also show a random population (red line on Figure 14), where we randomly placed 799 X-ray sources within the PHAT coverage and plotted the cumulative distribution in the same manner as the real X-ray sources. We repeated the

simulations 100 times and showed the 1σ with the red shaded region. It is evident that up until ~100 pc, the real distribution does not match the random one. This suggests that the real XRBs are not drawn from a random distribution, and the XRBs are preferentially situated close to the clusters. Beyond ~100 pc the two distributions were within 1σ . This may be because at larger distances the "signal" may be lost as XRBs flying away from their parent cluster can get closer to another cluster.

IV. CONCLUSIONS AND FUTURE WORK

We have obtained results of the x-ray sources in the PHAT region in Andromeda, which covers roughly 1/3 of Andromeda. Out of 799 X-ray sources within the PHAT coverage, 781 of them contain at least one counterpart. Most of the X-ray sources range at an age of 500 million years with very few younger than 50 million years. This indicates that most of the X-ray sources within M31 are HMXBs.

This finding is consistent with the analysis of the X-ray luminosity function. At least within the ~10^{35}-10^{38} erg/s range, we find that the slope of the X-ray luminosity function can be fitted with a power law with $\alpha = 1.7 \pm 0.1$. This power law is consistent with other spiral and starburst galaxies where HMXBs dominate the X-ray source population.

We also investigated the parent cluster candidates. We showed that at a distance smaller than ~100 pc, the XRBs are located closer to the clusters compared to a random placement. This suggests that these clusters are likely the parent clusters of their corresponding XRBs.

Going forward, we will apply a machine-learning an automated machine learning classification tool will be utilized to process all available data in the archives and provide a classification (and confidence level) for each source (which is beyond the scope of this work). This tool uses a training dataset of literature verified sources to learn from. The same machine learning approach will be applied to other nearby galaxies as well. We will then compare the results from several galaxies in our “neighborhood” and investigate how similar or different the X-ray source populations are.

REFERENCES

Dalcanton, J. J., Williams, B. F., Lang, D., Lauer, T. R., Kalirai, J. S., Seth, A. K., Dolphin, A. E., Rosenfield, P., Weisz, D. R., Bell, E. F., Bianchi, L., Meixner, M., Caldwell, N., Dong, H., Dorman, C. E., Gilbert, K. M., Girardi, L., Gogarten, S. M., Gordon, K. D., . . . Stanek, K. Z. (2012). THE PANCHROMATIC HUBBLE ANDROMEDA TREASURY. *The Astrophysical Journal Supplement Series*, *200*(2), 18. https://doi.org/10.1088/0067-0049/200/2/18

Rice, J., Rangelov, B., Prestwich, A., Chandar, R., Bichon, L., & Boldt, C. (2021). X-Ray Binaries in M51 I: Catalog and Statistics. *The Astrophysical Journal*, *922*(2), 178. https://doi.org/10.3847/1538-4357/ac22ac

De Meulenaer, P., Stonkute, R., & Vansevičius, V. (2017). Deriving physical parameters of unresolved star clusters. V. M 31 PHAT star clusters. *A&A*, *602*, A112. https://doi.org/10.1051/0004-6361/201730751

De Meulenaer, P., Narbutis, D., Mineikis, T., & Vansevičius, V. (2015). Deriving physical parameters of unresolved star clusters - III. Application to M 31 PHAT clusters. *Astronomy and Astrophysics*, *574*. https://doi.org/10.1051/0004-6361/201425121

Garner, R. (2021). Messier 31 (The Andromeda Galaxy). *NASA*. https://www.nasa.gov/feature/goddard/2017/messier-31-the-andromeda-galaxy

information@eso.org. (n.d.). *Red Giant*. ESA/Hubble | ESA/Hubble. https://www.esahubble.org/wordbank/red-giant/

scheme=AGLSTERMS.AglsAgent; corporateName=CSIRO Australia Telescope National Facility; address=PO Box 76 Epping NSW 1710 Australia; contact=+61 2 9372 4100 (phone),+61 2 9372 4310 (fax); jurisdiction=Commonwealth. (n.d.). *Types of Binary Stars*. https://www.atnf.csiro.au/outreach//education/senior/astrophysics/binary_types.html

Chandra X-ray Observatory - NASA's flagship X-ray telescope. (n.d.). https://chandra.harvard.edu/

Seward, F. D., & Charles, P. A. (2010). *Exploring the X-ray Universe*. Cambridge University Press.

Choudhuri, A. R. (2010). *Astrophysics for Physicists*. Cambridge University Press.

information@eso.org. (n.d.-a). *Hertzsprung-Russell Diagram*. www.eso.org. https://www.eso.org/public/images/eso0728c/

Roche-lobe | COSMOS. (n.d.). https://astronomy.swin.edu.au/cosmos/r/roche-lobe